ACS OMEGA

http://pubs.acs.org/journal/acsodf

Article

Interference Effect of Experimental Parameters on the Mercury Removal Mechanism of Biomass Char under an Oxy-Fuel Atmosphere

Yiming Zhu,*,§ Jingmao Wu,§ Hui Wang,* Jiajun Wang, Haotian Shen, and Zhanfeng Ying

Cite This: *ACS Omega* 2021, 6, 35124−35133

Read Online

ACCESS | Metrics & More | Article Recommendations | Supporting Information

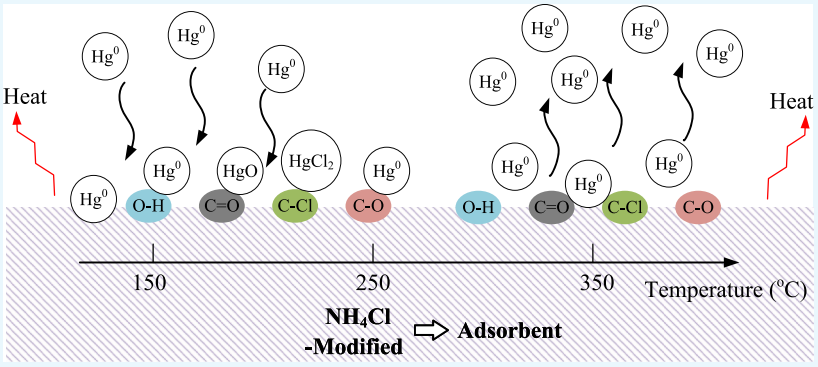

ABSTRACT: In this paper, the effect of temperature, adsorption bed height, and initial mercury concentration under oxy-fuel combustion on mercury adsorption by 1% NH_4Cl-modified biomass char was studied. Modification enriched the pore structure of biomass char and increased the number of surface functional groups. Higher temperature would lead to the destruction of van der Waals and reduce the adsorption efficiency, while the change of adsorption bed height had no obvious effect. Adsorption thermodynamics shows that the mercury removal process is a spontaneous exothermic process. The increase of initial mercury concentration would increase the driving force of mercury diffusion to the surface and improve the adsorption capacity. Meanwhile, three kinetic models including the intraparticle diffusion model, pseudo-first-order model, and pseudo-second-order model were applied to explore the internal mechanism of mercury adsorption by biomass char. The results showed that the pseudo-first-order model and pseudo-second-order model could accurately describe the adsorption process, which meant that the progress of external mass transfer played an important role in the adsorption of mercury while chemical adsorption should not be ignored. The intraparticle diffusion model indicated that internal diffusion was not the only step to control the entire adsorption process and did not have an inhibition on mercury removal. Higher initial mercury concentration would promote the external mass transfer progress and chemical adsorption progress. In addition, higher temperature inhibited the external mass transfer, which was not conducive to the adsorption of mercury.

1. INTRODUCTION

Global warming has become a huge threat and obstacle to human survival and development,[1,2] and coal-fired flue gas emissions are the biggest culprit of the greenhouse effect and China has become the largest carbon emitter in the world.[3] Carbon capture and storage (CCS) technology is a technology that collects CO_2 from large power plants and stores it in various ways to avoid its emission into the atmosphere.[4,5] Oxy-fuel combustion technology based on the recycling of CO_2 is considered to be the most promising advanced combustion technology.[6,7] At present, oxy-fuel combustion in a fluidized bed is an advanced combustion method widely used.[8−10] Compared with the traditional combustion mode, the flue gas composition of oxy-fuel combustion has changed greatly.[11,12]

In addition, the mercury content in the flue gas will increase due to the recirculation of the flue gas in the oxy-fuel combustion device. Mercury is a highly toxic pollutant with strong volatility, bioaccumulation, and environmental persistence.[13,14] Meanwhile, the high content of mercury will react with the metal in the device and cause serious safety hazards.[15] Therefore, mercury must be removed from oxy-fuel combustion flue gas whether from the point of view of

Received: October 28, 2021
Accepted: December 1, 2021
Published: December 13, 2021

environmental protection or safety. There are three main forms of mercury in coal-fired flue gas: gaseous mercury(Hg^0), gaseous oxidized mercury(Hg^{2+}), and particulate mercury-(Hg^P).[16] Hg^0 is the most difficult to capture because of its high volatility and low water solubility.[17] Hg^{2+} and Hg^P can be separately removed by existing wet desulfurization and dust removal devices in power plants.[18]

The mercury control technology of coal combustion includes precombustion mercury removal, in-combustion mercury removal, and postcombustion mercury removal.[19] The main means of precombustion mercury removal technology include coal preparation technology and coal washing technology.[20] Mercury removal in combustion mainly uses advanced combustion mode, which has been studied in the field of circulating fluidized adsorption beds.[21] Mercury removal after combustion includes mercury removal by the adsorbent and new mercury pollution control technology.[22,23]

At present, activated carbon injection (ACI) is the most mature and feasible technology for mercury removal in coal-fired power plants.[24,25] Scholars have carried out a lot of experiments and theoretical studies on mercury removal by activated carbon from coal-fired flue gas.[26−28] However, activated carbon is expensive and not suitable for large-scale commercial use. Nowadays, researchers have turned their attention to biomass.[29,30] Biomass char is an ideal adsorbent for mercury removal due to its low price, abundant surface functional groups, simple raw materials, and environmental protection.[31,32]

The parameters in the experiment will also have a great impact on the experimental results. Zhao et al.[33] showed that the change of Hg^0 removal efficiency with the increase of reaction temperature is non-monotonical. Wang et al.[34] showed that the increase of initial mercury concentration would promote the diffusion of mercury to the adsorbent surface. Shen et al.[35] showed that the efficiency of Hg^0 removal by the hierarchical sorbent was higher than that of conventional biochar by 40 to 65% at a temperature range from 80 to 180 °C. These results are closely related to the actual mercury removal in coal-power plants, while they are not comprehensive enough. In order to explore the inner mechanism of mercury, kinetic and thermodynamic models were used to analyze. Yang et al.[36] found that due to the mesoporous structure of the adsorbent, the intraparticle diffusion and the initial adsorption are not the rate control steps of Hg^0 capture. Zhong et al.[37] used a pseudo-second-order kinetic model to study the influence of mass and the gas flow rate of adsorbent on the adsorption performance. Ghasemi et al.[38] obtained through thermodynamic analysis that the increase of temperature is not conducive to the adsorption of mercury, and the kinetic study shows that the pseudo-second-order model can represent the adsorption mechanism of mercury.

It could be seen that at present, there are few research studies on the effect of adsorption bed height on mercury adsorption, and research on the effect of temperature, adsorption bed height, and initial mercury concentration on mercury adsorption efficiency was not comprehensive enough. In addition, most of the studies were conducted in an ordinary atmosphere, so it was necessary to explore the influence of experimental parameters on mercury adsorption in an oxygen-enriched atmosphere and determine the best parameters in the experiment. Meanwhile, it was also necessary to use a kinetic model to verify and analyze the adsorption mechanism to verify the correctness of parameter selection.

2. RESULTS AND DISCUSSION

2.1. Characterization of Biomass Char. After the selection of biomass raw materials, we first carried out industrial analysis and thermogravimetric analysis on the raw materials. Then, we modified the biomass char with 1% NH_4Cl solution and analyzed the modified biomass char by means of scanning electron microscopy (SEM), Fourier transform infrared (FTIR), and Brunauer−Emmett−Teller (BET). The biomass char adsorbent used in this paper was also used in another published paper of the author.[35] Because it has been described in detail in the paper mentioned above, it will not be necessary to be described here and the content of this part will be attached to the Supporting Information.

2.2. Effect of Temperature on Removal of Mercury. In this experiment, three different adsorption temperatures including 150, 250, and 350 °C were selected to study the effect of temperature on mercury adsorption. The adsorption bed height was 3 mm, and initial mercury concentration was 54.40 $\mu g/m^3$.

First of all, we did the comparative experiment of mercury in an oxy-fuel atmosphere and ordinary combustion atmosphere at 150 °C. It can be seen from Figure 1 that the mercury

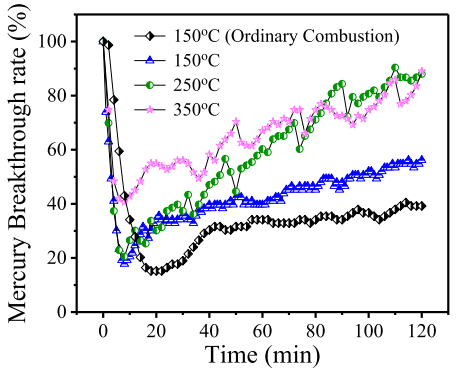

Figure 1. Effect of temperature on mercury adsorption efficiency.

breakthrough rate in the ordinary combustion atmosphere is significantly lower than that in the oxy-fuel atmosphere. At the same time, it can be seen from Figure 2 that the mercury uptake in the ordinary combustion atmosphere is 193.02 $\mu g/g$, while that in the oxy-fuel atmosphere is 149.93 $\mu g/g$. It can be seen that the oxy-fuel gas is not conducive to the adsorption of mercury by the adsorbent, and the main reason may be that Hg^0 (2.97 Å) and CO_2 (3.30 Å) have similar kinetic diameters,

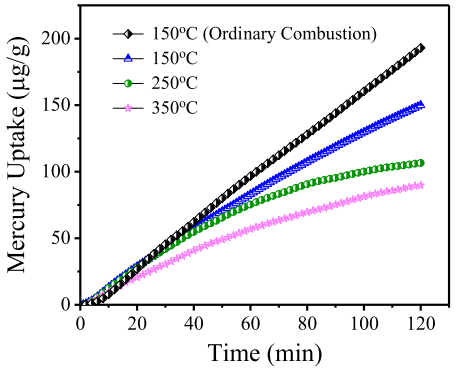

Figure 2. Effect of temperature on mercury uptake.

https://doi.org/10.1021/acsomega.1c06038
ACS Omega 2021, 6, 35124−35133

Table 1. Parameters from Adsorption Thermodynamic

ln k_0	E_a (KJ/mol)	ΔS (J/mol·K)	ΔH (KJ/mol)	ΔG (KJ/mol)		
				150 °C	250 °C	350 °C
−13.99	−16.23	−3.30	−4.66	−3.58	−2.93	−2.60

which make their adsorption behavior in pores similar. Therefore, Hg^0 competes with CO_2 for physical adsorption.[39,40] It can be seen from Figures 1 and 2 that when the temperature rose from 150 to 350 °C, the mercury breakthrough rate increased and the mercury uptake decreased. The results showed that high temperature could inhibit the adsorption of mercury.

2.2.1. Adsorption Thermodynamics. Activation energy was needed in the mercury removal process. Based on the k_2 of the pseudo-second-order kinetic model, the following eq 1 can be obtained by the Arrhenius equation.[41]

$$\ln k_2 = -\frac{E_a}{RT} + \ln k_0 \quad (1)$$

Where k_2 is the kinetic constant of the pseudo-second-order kinetic equation, g/(μg min); k_0 is the Arrhenius equation factor; R is the molar gas constant, 8.314 J/(mol K); E_a is the adsorption activation energy, kJ/mol; and T is the reaction temperature, K.

The value of E_a was between 0 and −4 kJ/mol for physical adsorption and −40 to −800 kJ/mol for chemical adsorption.[42] It can be seen in Table 1 that the E_a was in the range of −4 to −40 kJ/mol, which shows that the mercury removal process had both physical adsorption and chemical adsorption.

The adsorption thermodynamic parameters include enthalpy (ΔH), entropy (ΔS), and Gibbs free energy (ΔG). ΔG determines whether the adsorption process is spontaneous, ΔH determines whether the adsorption process is exothermic or endothermic, ΔS reflects the chaos of the adsorption process, and the adsorption thermodynamic parameters can be obtained by eqs 2 and 3.[43,44]

$$\Delta G = -RT \ln K \quad (2)$$

$$\Delta G = \Delta H - T\Delta S \quad (3)$$

where K is equal to q_e/C_e; q_e is the cumulative adsorption capacity of the adsorbent for Hg^0 at equilibrium time, (μg/g); and C_e is the equilibrium concentration of Hg^0 at the outlet of the adsorption reactor, (μg/m^3).

From Table 1, the reason why ΔS is negative may be that mercury molecules lose randomness when adsorbed to the adsorbent surface.[45] ΔH is negative, which indicates that the mercury adsorption process is exothermic. Generally, the chemical adsorption process is endothermic and the physical adsorption process is exothermic, but the reaction process between mercury and active chlorine atoms is exothermic.[46,47] Therefore, the mercury removal process is controlled by physical adsorption and chemical adsorption, and low temperature is conducive to mercury removal. Moreover, ΔG is negative suggesting that the mercury adsorption process is spontaneous. The absolute value of ΔG decreases with the increase of temperature, which indicates that mercury is not easy to adsorb on the surface of the adsorbent with the increase of temperature.[42] It further demonstrates that the increase of temperature is unfavorable to the mercury removal process.

Above all, the reasons for the negative effect of temperature on mercury removal efficiency may be that the adsorption of mercury in the initial stage on corn straw char was the main physical adsorption process,[48] which was mainly caused by the van der Waals force between molecules.[49] Moreover, the limitation of high temperature on the physical adsorption of Hg^0 will inhibit the chemical adsorption of Hg^0.[50] In this process, the uptake was relatively weak and exothermic, so the uptake decreased with the increase of adsorption temperature. In the dynamic equilibrium of adsorption and desorption of elemental mercury, a higher temperature was more favorable for desorption,[51,52] thus leading to a higher breakthrough rate.

2.3. Effect of Adsorption Bed Height on Removal of Mercury. In this experiment, three different adsorption bed heights of 3, 5, and 7 mm were selected at the temperature of 150 °C with an initial mercury concentration of 54.4 μg/m^3 to explore the influence of adsorption bed height on mercury adsorption. It can be seen from Figure 3 that the three mercury breakthrough rate curves were almost coincident, with slightly different values but the overall trend remained the same. From Figure 4, the mercury uptake ranged from 147.83 to 144.21

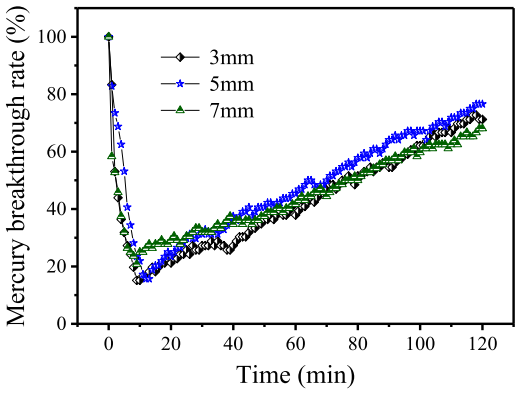

Figure 3. Effect of adsorption bed height on mercury adsorption efficiency.

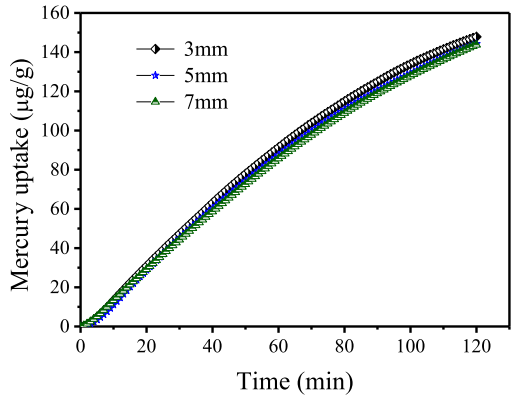

Figure 4. Effect of adsorption bed height on mercury adsorption efficiency.

https://doi.org/10.1021/acsomega.1c06038
ACS Omega 2021, 6, 35124−35133

μg/g and to 143.75 μg/g, and there was basically no difference in the mercury uptake corresponding to the three different adsorption bed heights. It was mainly because of the fact that the initial mercury concentration, adsorption temperature, and other influencing factors remain unchanged and the mercury breakthrough rate under various working conditions were basically the same, so there would be no difference in the cumulative mercury uptake. Therefore, the adsorption bed height had little effect on mercury adsorption.

2.4. Effect of Initial Mercury Concentration on Removal of Mercury. In this experiment, the effects of four different mercury concentrations on the adsorption were studied, including 28, 36.8, 54.4, and 61.6 μg/m^3, respectively. The adsorption temperature was 150 °C and adsorption bed height was 3 mm. It can be seen from Figure 5 that when the

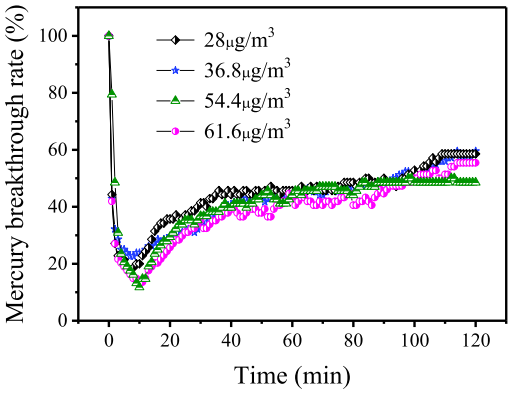

Figure 5. Effect of initial mercury concentration on mercury adsorption efficiency.

mercury content increased from 28 to 54.4 μg/m^3, the breakthrough rate of mercury decreased continuously. When the initial mercury concentration increased to 61.6 μg/m^3, it was found that the minimum breakthrough rate increased to a certain extent, which indicated that the adsorption efficiency decreases to a certain extent. As can be seen from Figure 6,

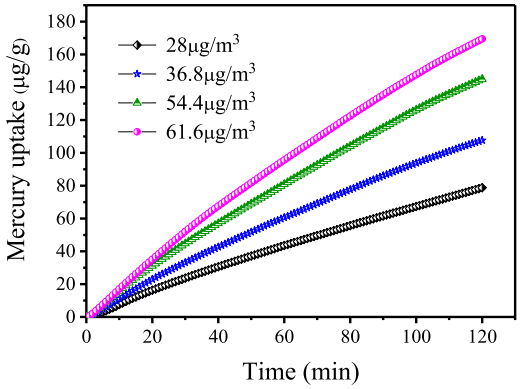

Figure 6. Effect of initial mercury concentration on mercury uptake.

with the increase of initial mercury concentration, the mercury uptake also increased, ranging from 78.79 to 107.64 and 144.97 and 169.43 μg/g, respectively. This was mainly because the increase of initial mercury concentration could improve the mercury diffusion rate on the surface of corn straw char, making it easier for mercury to enter into the surface of the adsorbent and improve the external mass transfer rate.[53] Meanwhile, the increase of mercury concentration also increased the uptake of mercury, leading to the occupation of active sites and vacancies, so the adsorption efficiency was relatively reduced. Therefore, in a certain range, the increase of mercury concentration could promote the adsorption of mercury.

2.5. Kinetic Analysis of Mercury Adsorption with the Intraparticle Diffusion Model. In Figures 7−9, it can be

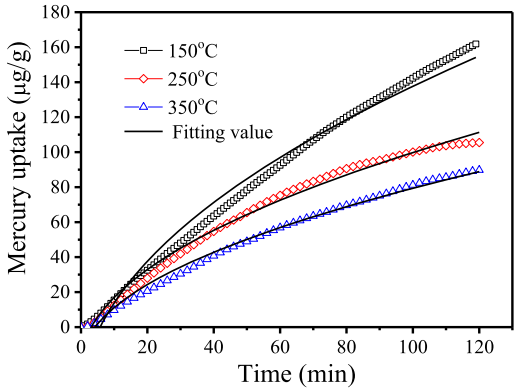

Figure 7. Intraparticle diffusion model at different adsorption temperatures.

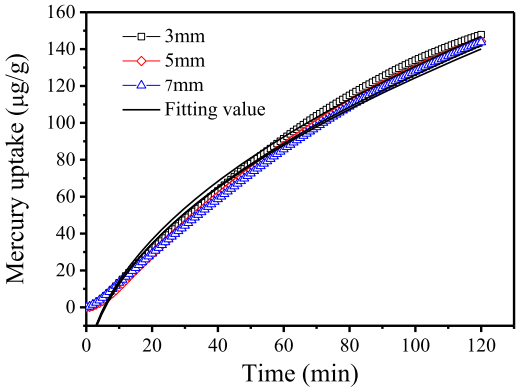

Figure 8. Intraparticle diffusion model at different adsorption bed heights.

seen that the fitting curves under oxy-fuel conditions were all not consistent well with the experimental results and did not pass through the origin point which showed that the

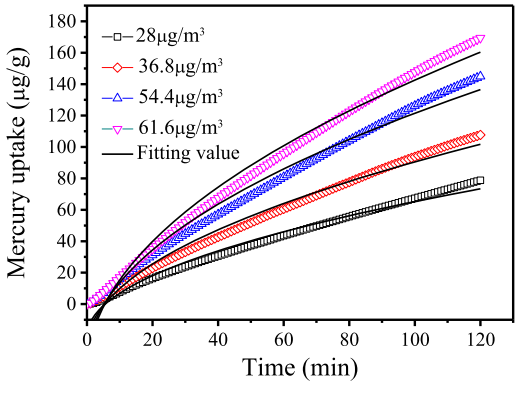

Figure 9. Intraparticle diffusion model at different initial mercury concentrations.

https://doi.org/10.1021/acsomega.1c06038
ACS Omega 2021, 6, 35124−35133

intraparticle diffusion model is not the only step to control the adsorption process. Moreover, as can be seen from Table 2, all R_2 were less than 0.99, which indicated that internal diffusion was not the only step to control the entire adsorption process.

Table 2. Parameters and Correlation Coefficient Obtained from the Intraparticle Diffusion Kinetic Model

factor	condition	k_p (μg/g min$^{1/2}$)	C (μg/g)	R^2
temperature (°C)	150	18.09	−43.21	0.98429
	250	12.09	−21.20	0.98300
	350	9.961	−20.25	0.97619
adsorption bed height (mm)	3	16.98285	−39.1391	0.98325
	5	16.57104	−39.5634	0.98207
	7	16.27170	−38.1871	0.98066
initial mercury concentration (μg/m^3)	28.0	8.53405	−20.1204	0.97645
	36.8	11.76257	−27.1273	0.97728
	54.4	15.74812	−36.0116	0.97594
	61.6	18.57738	−43.1422	0.97749

The adsorption of mercury was mainly divided into two stages, which were surface adsorption and internal diffusion adsorption. The initial adsorption stage was surface adsorption, and the active center of the biomass char surface and Hg^0 could be easily adsorbed.[54] When surface active sites were occupied, the adsorption entered the second stage that was the diffusion adsorption in the pore.

With the increase of temperature, k_p decreased continuously and the values of correlation coefficient R^2 were all below 0.99, indicating that internal diffusion has had a restrictive effect. At 150 °C, the k_p value is the largest, indicating that the intraparticle diffusion effect is most obvious at this temperature. At low temperature, the driving force of chemical adsorption is not enough, mainly physical adsorption. It can be seen from Table S2 (Supporting Information) that the average pore diameter of the modified biomass coke is 1.570 nm, which belongs to the micropore level, so the diffusion resistance in the particle is mainly the configuration diffusion resistance in micropores.[55] The k_p of different adsorption bed heights ranged from 16.98285 to 16.27170, which meant the adsorption rate maintained a similar level, indicating that internal diffusion did not have an inhibition on mercury removal. In addition, when R^2 values were almost below 0.985, the removal effect of internal diffusion on mercury did not show a significant correlation with the adsorption bed height. Meanwhile, the change of R_2 did not show obvious correlation with the change of initial mercury concentration, which was consistent with the conclusion of the experiment, indicating that the internal diffusion control has no effects. With the initial mercury concentration increase, k_p increased continuously, and the adsorption rate remained high, indicating that internal diffusion has no restrictive effect. Therefore, it could be summarized that the adsorption rate was very fast in the initial stage of adsorption, which indicated that surface adsorption occurred in the initial stage of adsorption.

2.6. Kinetic Analysis of Mercury Adsorption with the Pseudo-First-Order Kinetic Model. As shown in Figures 10−12, it can be seen that the fitting curves all fitted well with experimental data, which meant that the pseudo-first-order model could describe the adsorption process well, indicating that the external mass transfer process had an obvious effect on

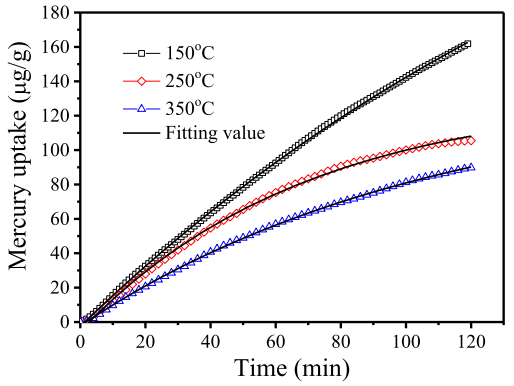

Figure 10. Pseudo-first-order model at different adsorption temperatures.

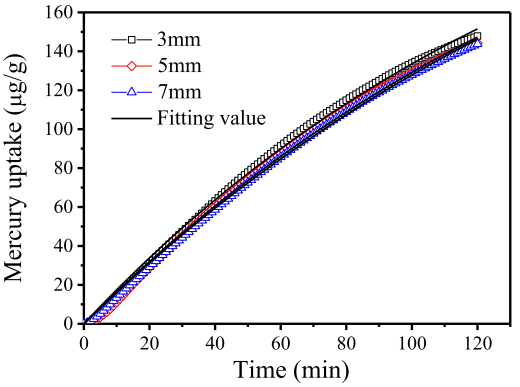

Figure 11. Pseudo-first-order kinetic model at different adsorption bed heights.

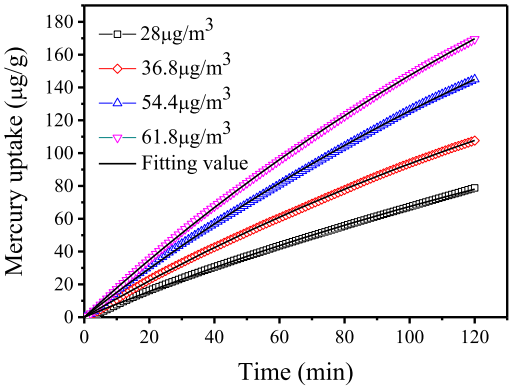

Figure 12. Pseudo-first-order kinetic model at different initial mercury concentrations.

the adsorption process. Meanwhile, the R_2 values in Table 3 were all above 0.99, which agreed with the experimental results.

From Table 3, it can be seen that the k_1 of adsorption temperature ranged from 0.00327 to 0.00799, and the increase of k_1 was quite large, indicating that the temperature change had a great influence on the external mass transfer process, which was consistent with the experimental results mentioned above. When the temperature increased from 150 to 350 °C, the R^2 kept decreasing, which indicated that the external mass transfer process had a weakening effect on the adsorption process. This phenomenon may because of the fact that the increase of temperature improved the driving force to

https://doi.org/10.1021/acsomega.1c06038
ACS Omega 2021, 6, 35124−35133

Table 3. Parameters and Correlation Coefficient Obtained from the Pseudo-First-Order Kinetic Model

factors	condition	q_e (μg/g)	k_1 (min^{-1})	R^2
temperature (°C)	150	464.7574	0.00327	0.99964
	250	143.1553	0.01200	0.99901
	350	147.1038	0.00799	0.99633
adsorption bed height (mm)	3	284.8981	0.00632	0.99782
	5	300.7241	0.00561	0.99881
	7	309.4448	0.00533	0.99742
initial mercury concentration (μg/m^3)	28	205.5150	0.00398	0.99962
	36.8	260.8095	0.00444	0.99981
	54.4	359.0113	0.00431	0.99964
	61.6	411.3625	0.00443	0.9998

overcome the mass transfer resistance between the gas and solid phase,[56] but when the temperature is too high, the molecules will move violently, which will cause the desorption of the adsorbate.[57] With the adsorption bed height increasing, the k_1 ranged from 284.8981 to 309.4448 and the R^2 ranged from 0.99782 to 0.99742. The changes of k_1 and R^2 with adsorption bed height were not obvious, which meant that the change of adsorption bed height had little effect on external mass transfer. With the initial mercury concentration increase, R_2 also kept increasing and k_1 also increased, ranging from 0.00398 to 0.00443, indicating that the increase of initial mercury concentration was conducive to the external mass transfer process, and this was in line with Liu et al.[58] The result of the pseudo-first-order model indicated that the mass transfer played an important role in the adsorption process, which was also consistent with Sriram et al.'s[59] conclusion.

2.7. Kinetic Analysis of Mercury Adsorption with the Pseudo-Second-Order Kinetic Model. In Figures 13−15,

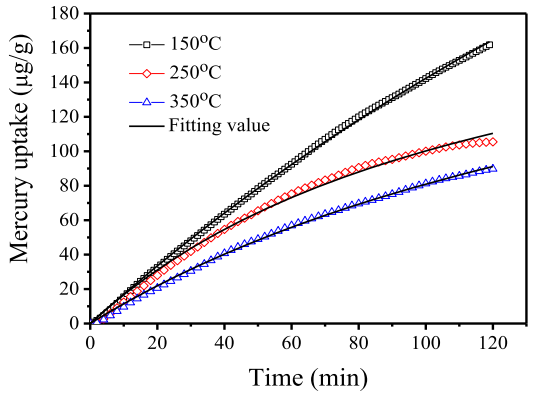

Figure 13. Pseudo-second-order model at different adsorption temperatures.

the fitting curves of the pseudo-second-order model all fitted well with experimental data, which indicated that the pseudo-second-order model could be used to describe the adsorption process.

When the temperature was 150 °C, the q_e and k_2 were the largest. With the temperature increase, k_2 decreased, ranging from 1.804 to 1.750 and to 1.202, respectively, indicating that the correlation became worse. The effect of temperature rise on the demercuration performance of biomass char is mainly manifested in the acceleration of the chemical reaction rate between the surfactant and mercury to the enhancement of

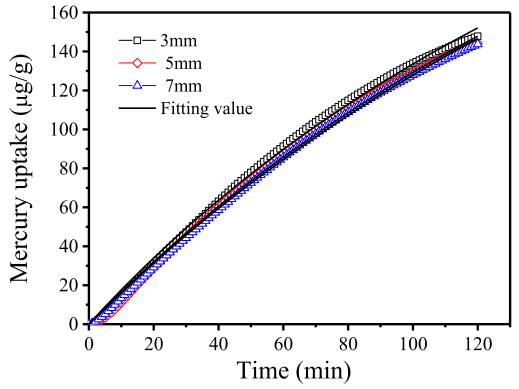

Figure 14. Pseudo-second-order kinetic model at different adsorption bed heights.

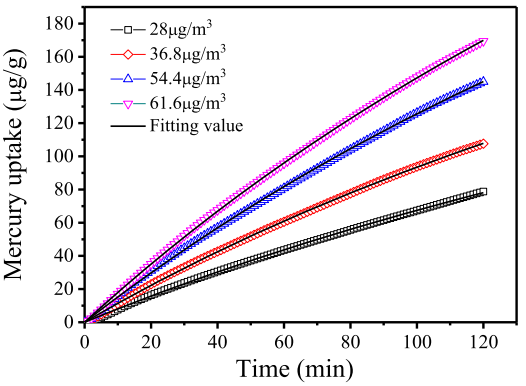

Figure 15. Pseudo-second-order kinetic model at different initial mercury concentrations.

chemical adsorption.[60] Too high temperature may lead to the desorption and decomposition of adsorbed mercury[36,61] and even decompose the oxygen-containing functional groups,[60] thus reducing the removal of mercury by the adsorbent. Moreover, q_e increased with the adsorption bed height increased, ranging from 500.000 to 555.556 and 578.743, respectively. The value of k_2 decreased from 1.8238 to 1.7027 and 1.5133, respectively. These data indicated that the change of adsorption bed height did not have an obvious effect on mercury adsorption. When the initial mercury concentration increased from 28 to 61.6 μg/m^3, the q_e increased from 371.7472 to 740.7407, and k_2 ranged from 0.8247 to 1.8395, which showed that the increase of mercury concentration promoted chemical adsorption progress.Table 4 Generally, the correlation coefficient was very similar to that of external mass transfer, which was fitted by pseudo-first-order model, indicating that the chemical adsorption process in the adsorption of mercury could not be ignored.[62]

3. CONCLUSIONS

In this paper, corn straw char was selected and modified with 1% NH_4Cl solution. The results showed that the surface pore structure was developed, and there were many new pore and mesoporous structures. Meanwhile, the number of surface functional groups was increased, which improved the uptake of corn stalk (CS) char. Higher temperature will lead to the destruction of van der Waals force and the redesorption of mercury, which causes the decrease of adsorption efficiency. Adsorption thermodynamics shows that the adsorption process

https://doi.org/10.1021/acsomega.1c06038
ACS Omega 2021, 6, 35124−35133

Table 4. Parameters and Correlation Coefficient Obtained from the Pseudo-Second-Order Kinetic Model

factor	condition	q_e (μg/g)	k_2 (μg/g min)	R^2
temperature (°C)	150	769.231	1.804	0.99947
	250	227.273	1.750	0.99872
	350	250.000	1.202	0.99400
adsorption bed height (mm)	3	500.000	1.8238	0.99747
	5	555.556	1.7027	0.99715
	7	578.743	1.5133	0.99863
initial mercury concentration (μg/m^3)	28	371.7472	0.8247	0.99962
	36.8	467.2897	1.1683	0.99645
	54.4	645.1613	1.5608	0.99728
	61.6	740.7407	1.8395	0.98594

is controlled by both physical adsorption and chemical adsorption, and the mercury removal process is a spontaneous exothermic process, low temperature is conducive to mercury removal. The change of adsorption bed height has no effect on the adsorption efficiency of mercury. In a certain range, the increase of mercury concentration in the inlet will increase the external mass transfer rate, thus promoting the adsorption of mercury.

The fitting results of the pseudo-second-order model indicated that chemical adsorption dominated the mercury adsorption by biomass char while external mass transfer could not be ignored as obtained by the pseudo-first-order model. Results of the intraparticle diffusion model showed that internal diffusion was not the only step to control the adsorption progress. The increase of initial mercury concentration promoted the internal diffusion, external mass transfer, and chemisorption process. The increase of temperature inhibited the internal diffusion and external mass transfer, which is not conducive to adsorption. The external mass transfer rate and chemical reaction rate did not change obviously under different adsorption bed heights.

4. EXPERIMENT SECTION

4.1. Adsorbent and Modification. The biomass material was CS collected from Nanjing, China. First, the biomass raw materials were subjected to a pretreatment process such as air drying, crushing, and sieving to prepare biomass raw materials. Through sieving, the raw materials had a particle diameter of less than 1 mm, ranging from 100 to 150 mesh and pyrolysis at 600 °C for 10 min. After that, we continued to pass the biomass char through the 100−150 mesh sieve again and obtained biomass char of particles directly in the range of 0.1−0.2 mm. Then, the biomass char was impregnated by 1% NH_4Cl and stirred continuously for 24 h, then it was put in a 40 °C oven for drying, and finally we obtained the modified corn straw char. NH_4Cl is selected considering the important role of chlorine containing functional groups in mercury oxidation and the combined removal of NO_x by NH_3 produced by pyrolysis of NH_4Cl at high temperature in an actual combustion atmosphere of a coal power plant.[63,64] CSM stands for the CS char modified by 1% NH_4Cl.

4.2. Experimental Platform and Procedure. The experimental platform is shown in Figure 16. It mainly includes a mercury generation system, gas distribution system, fixed-bed reactor system, and tail gas treatment system. Hg^0 is generated from a mercury permeation device (VICI Metronics Inc, USA), which is designed to maintain a constant release ratio of Hg^0 vapor at the specified temperature. In the experiment, 50 mg of corn stalk char was spread on the surface of the adsorption bed in a glass tube, and the total flow of simulated flue gas was 2 L/min. CO_2 is used to carry mercury, and the flow rate is 200 mL/min. The basic atmosphere in an oxy-fuel atmosphere is 70% CO_2 + 6% O_2 while the balanced gas is Ar. The ordinary combustion atmosphere is 12% CO_2 + 6% O_2. The mercury measuring instrument was QM-208B based on the CVAAS method, whose measuring range and sensitivity were 0.1−100 and 0.03 μg/m^3, respectively. Table 5 shows the experiment conditions, covering the temperature range, gas flow resistance, and inlet mercury concentration of the actual coal-fired power plant.

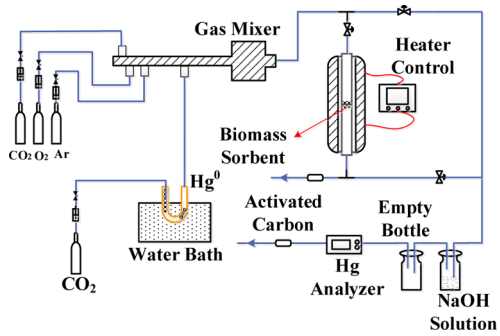

Figure 16. Diagram of the small fixed-bed reaction platform.

4.3. Evaluation of the Adsorbent. *4.3.1. Mercury Breakthrough Rate.* The mercury breakthrough rate is the ratio of mercury concentration after adsorption to mercury concentration before adsorption and is given by eq 4

$$\eta = \frac{C_{out}}{C_{in}} \times 100\% \tag{4}$$

where η is the mercury breakthrough rate; C_{out} is the mercury concentration in the flue gas after passing through the quartz tube reactor, μg/m^3; and C_{in} is the concentration of mercury in the simulated flue gas before entering the quartz tube reactor, μg/m^3.

4.3.2. Mercury Uptake. The cumulative adsorption amount of mercury units can reflect the uptake of mercury per unit mass of the adsorbent, which is given by eq 5

$$Q = \int_0^t \left(1 - \frac{C}{C_0}\right) q \, dt \; C_0/m \approx \sum_{i=0}^{n} \left(1 - \frac{C_i + C_{i+1}}{2C_0}\right) q \Delta t C_0/m \tag{5}$$

where Q is the amount of mercury adsorption, which refers to the amount of mercury adsorption per unit mass of the adsorbent at 0−t μg/g; C is the mercury concentration at the outlet of the fixed adsorption bed during the test period, μg/m^3; C_i is the mercury concentration at the outlet of the fixed adsorption bed at the time point, μg/m^3; C_{i+1} is the mercury concentration at the outlet of the fixed adsorption bed at the i + 1st time point, μg/m^3; Δt is the sampling interval, and the sampling interval in this experiment is 2 min; q is the total gas flow rate in the experiment, m^3/min; and m is the mass of the adsorbent, g.

4.4. Kinetic Models. *4.4.1. Intraparticle Diffusion Model.* The intraparticle diffusion model is commonly used to

https://doi.org/10.1021/acsomega.1c06038
ACS Omega 2021, 6, 35124−35133

Table 5. Experimental Conditions

code	initial Hg^0 concentration ($\mu g\ m^{-3}$)	adsorption bed height (mm)	simulated flue gas	adsorption temperature (°C)
1	54.4	3	12% CO_2 + 6% O_2 + Ar	150
2	54.4	3	70% CO_2 + 6% O_2 + Ar	150
3	54.4	3	70% CO_2 + 6% O_2 + Ar	250
4	54.4	3	70% CO_2 + 6% O_2 + Ar	350
5	54.4	3	70% CO_2 + 6% O_2 + Ar	150
6	54.4	5	70% CO_2 + 6% + Ar	150
7	54.4	7	70% CO_2 + 6% O_2 + Ar	150
8	28.0	3	70% CO_2 + 6% O_2 + Ar	150
9	36.8	3	70% CO_2 + 6% O_2 + Ar	150
10	54.4	3	70% CO_2 + 6% O_2 + Ar	150
11	61.6	3	70% CO_2 + 6% O_2 + Ar	150

describe the internal diffusion process of pores during solid adsorption. The model considers the diffusion effect by using a partial differential equation describing the diffusion of spherical particles. The equation is expressed as follows[65,66]

$$q_t = k_p t^{1/2} + C \tag{6}$$

where q_t is the cumulative mercury adsorption per unit mass of the adsorbent, $\mu g/g$; k_p is the intraparticle diffusion rate constant, $\mu g/(g\ min^{1/2})$; t is the reaction time, min; and C is a constant related to the thickness of the boundary layer, which represents the extent of the boundary layer effect, $\mu g/g$.

4.4.2. Pseudo-First-Order Kinetic Model. The pseudo-first-order model uses the concentration difference as the driving force to describe the mass transfer process. If the experimental data and the calculated data could agree well, then, we could reach the conclusion that the external mass transfer had an obvious control effect on the adsorption process.[67] The pseudo-first-order kinetic equation is shown in eq 7

$$\frac{dq_t}{dt} = k_1(q_e - q_t) \tag{7}$$

Integrated by the boundary condition $t = 0$, $q_t = 0$; $t = t$, $q_t = q_t$, the eq 8 is transformed to

$$q_t = q_e(1 - e^{-k_1 t}) \tag{8}$$

where q_e is the equilibrium adsorption capacity, $\mu g/g$; and k_1 is the pseudo-first-order adsorption rate constant, min^{-1}.

4.4.3. Pseudo-Second-Order Kinetic Model. The pseudo-second-order model, which is based on the Langmuir adsorption isotherm equation, contains all processes of adsorption including external mass transfer, intraparticle diffusion, and surface adsorption. Among them, the formation of chemical bonds is the main factor affecting the pseudo-second-order kinetic adsorption. Therefore, it is used as the control step of the adsorption rate.[68] The equation is shown in eq 9

$$\frac{dq_t}{dt} = k_2(q_e - q_t)^2 \tag{9}$$

while boundary conditions are $t = 0$, $q_t = 0$; $t = t$, $q_t = q_t$

$$q_t = \frac{t}{\frac{1}{k_2 q_e^2} + \frac{t}{q_e}} \tag{10}$$

where q_e is the equilibrium absorbed amount, $\mu g/g$; q is the equilibrium absorbed amount at time t, $\mu g/g$; t is the absorbed time, min; and k_2 is the kinetic constant of the pseudo-second-order kinetic equation, $g/(\mu g\ min)$.

■ ASSOCIATED CONTENT

Supporting Information

The Supporting Information is available free of charge at https://pubs.acs.org/doi/10.1021/acsomega.1c06038.

Characterization data of biomass char include industrial analysis of raw material; TGA analysis of biomass char; FTIR analysis of CS char before and after 1% NH_4Cl modification; pore structure analysis of biomass char before and after 1% NH_4Cl modification; and SEM analysis of biomass char before and after 1% NH_4Cl modification (PDF)

■ AUTHOR INFORMATION

Corresponding Authors

Yiming Zhu − *School of Energy and Power Engineering, Nanjing University of Science and Technology, Nanjing 210094, China*; Email: ymzhu@njust.edu.cn

Hui Wang − *School of Energy and Power Engineering, Nanjing University of Science and Technology, Nanjing 210094, China*; orcid.org/0000-0001-7685-8482; Email: wanghui22@njust.edu.cn

Authors

Jingmao Wu − *School of Energy and Power Engineering, Nanjing University of Science and Technology, Nanjing 210094, China*

Jiajun Wang − *School of Energy and Power Engineering, Nanjing University of Science and Technology, Nanjing 210094, China*

Haotian Shen − *Nanjing Institute of Future Energy System, Institute of Engineering Thermodynamics, Chinese Academy of Sciences, Nanjing 210000, China*

Zhanfeng Ying − *School of Energy and Power Engineering, Nanjing University of Science and Technology, Nanjing 210094, China*

Complete contact information is available at: https://pubs.acs.org/10.1021/acsomega.1c06038

Author Contributions

[§]Y.Z. and J. Wu contributed equally.

Notes

The authors declare no competing financial interest.

https://doi.org/10.1021/acsomega.1c06038
ACS Omega 2021, 6, 35124−35133

■ ACKNOWLEDGMENTS

This work was supported by the National Natural Science Foundation of China (51706104); the Natural Science Foundation of Jiangsu Province (grant no. BK20180479); the Peak of the Six Talents Program of Jiangsu Province (XNY-026); the China Postdoctoral Science Foundation (grant no. 2020M681611); the Postgraduate Research & Practice Innovation Program of Jiangsu Province (SJCX21_0130); and the Open Fund for Large-scale Equipment of NUST.

■ REFERENCES

(1) Hughes, T. P.; Kerry, J. T.; Baird, A. H.; Connolly, S. R.; Chase, T. J.; Dietzel, A.; Hill, T.; Hoey, A. S.; Hoogenboom, M. O.; Jacobson, M.; Kerswell, A.; Madin, J. S.; Mieog, A.; Paley, A. S.; Pratchett, M. S.; Torda, G.; Woods, R. M. Global warming impairs stock−recruitment dynamics of corals. *Nature* **2019**, *568*, 387−390.

(2) Jin, C.; Sun, J.; Chen, Y.; Guo, Y.; Han, D.; Wang, R.; Zhao, C. Sawdust wastes-derived porous carbons for CO_2 adsorption. Part 1. Optimization preparation via orthogonal experiment. *Sep. Purif. Technol.* **2021**, *276*, 119270.

(3) Zhao, Y.; Yang, J.; Ma, S.; Zhang, S.; Liu, H.; Gong, B.; Zhang, J.; Zheng, C. Emission controls of mercury and other trace elements during coal combustion in China: a review. *Int. Geol. Rev.* **2018**, *60*, 638−670.

(4) Ding, M.; Flaig, R. W.; Jiang, H.-L.; Yaghi, O. M. Carbon capture and conversion using metal−organic frameworks and MOF-based materials. *Chem. Soc. Rev.* **2019**, *48*, 2783−2828.

(5) Bai, S.; Sun, J.; Zhou, Z.; Bu, C.; Chen, X.; Yang, Y.; Wang, R.; Guo, Y.; Zhao, C.; Liu, W. Structurally improved, TiO_2-incorporated, CaO-based pellets for thermochemical energy storage in concentrated solar power plants. *Sol. Energy Mater. Sol. Cells* **2021**, *226*, 111076.

(6) Nguyen, H. K.; Moon, J. H.; Jo, S. H.; Park, S. J.; Bae, D. H.; Seo, M. W.; Ra, H. W.; Yoon, S.-J.; Yoon, S.-M.; Lee, J. G.; Mun, T.-Y.; Song, B. Ash characteristics of oxy-biomass combustion in a circulating fluidized bed with kaolin addition. *Energy* **2021**, *230*, 120871.

(7) Zhang, Q.; Chen, G.; Deng, H.; Wen, X.; Wang, F.; Zhang, A.; Sheng, W. Experimental and numerical study of the effects of oxygen-enriched air on the laminar burning characteristics of biomass-derived syngas. *Fuel* **2021**, *285*, 119183.

(8) Wang, X.; Zhong, Z.; Jin, B. Experimental Evaluation of Biomass Medium-Temperature Gasification with Rice Straw as the Fuel in a Bubbling Fluidized Bed Gasifier. *Int. J. Chem. React. Eng.* **2019**, *18*, 20190147.

(9) Wu, Y.; Liu, D.; Duan, L.; Ma, J.; Xiong, J.; Chen, X. Three-dimensional CFD simulation of oxy-fuel combustion in a circulating fluidized bed with warm flue gas recycle. *Fuel* **2018**, *216*, 596−611.

(10) Wu, Y.; Liu, D.; Zheng, D.; Ma, J.; Duan, L.; Chen, X. Numerical simulation of circulating fluidized bed oxy-fuel combustion with Dense Discrete Phase Model. *Fuel Process. Technol.* **2019**, *195*, 106129.

(11) Wang, H.; Duan, Y.; Ying, Z.; Xue, Y. Effects of SO_2 on Hg Adsorption by Activated Carbon in O_2/CO_2 Conditions. Part 1: Experimental and Kinetic Study. *Energy Fuels* **2018**, *32*, 10773−10778.

(12) Moon, J.-H.; Jo, S.-H.; Park, S. J.; Khoi, N. H.; Seo, M. W.; Ra, H. W.; Yoon, S.-J.; Yoon, S.-M.; Lee, J.-G.; Mun, T.-Y. Carbon dioxide purity and combustion characteristics of oxy firing compared to air firing in a pilot-scale circulating fluidized bed. *Energy* **2019**, *166*, 183−192.

(13) Budnik, L. T.; Casteleyn, L. Mercury pollution in modern times and its socio-medical consequences. *Sci. Total Environ.* **2019**, *654*, 720−734.

(14) Dong, L.; Wang, H.; Huang, Y.; Zha, J.; Cheng, H.; Liu, L.; Zhu, Z.; Chen, H.; Ding, S.; Wang, S. gamma-Fe_2O_3 decorated attapulgite composite modified with $CuCl_2$ as magnetically separable sorbents for Hg^0 removal from coal combustion flue gas. *Chem. Eng. J.* **2021**, *408*, 127888.

(15) Yang, J.; Zhu, W.; Zhang, S.; Zhang, M.; Qu, W.; Li, H.; Zeng, Z.; Zhao, Y.; Zhang, J. Role of flue gas components in Hg^0 oxidation over $La_{0.8}Ce_{0.2}MnO_3$ perovskite catalyst in coal combustion flue gas. *Chem. Eng. J.* **2019**, *360*, 1656−1666.

(16) Shen, F.; Liu, J.; Dong, Y.; Wu, D.; Gu, C.; Zhang, Z. Elemental mercury removal from syngas by porous carbon-supported $CuCl_2$ sorbents. *Fuel* **2019**, *239*, 138−144.

(17) Zheng, H.; Chen, G.; Zhang, A.; Tan, Z.; Wang, R.; Wang, H.; Mei, Y.; Zhang, X.; Ran, J. Enhanced photocatalytic activity of $Bi_{24}O_{31}Br_{10}$ microsheets constructing heterojunction with AgI for Hg^0 removal. *Sep. Purif. Technol.* **2021**, *262*, 118296.

(18) Liu, H.; Chen, Y.; Gao, T.; Yang, G.; Wang, Y.; Zhou, Y.; Yang, J.; Zhao, Y.; Guo, X.; Zhang, J. Elemental mercury removal from flue gas using modified tonstein: Performance of adsorbent injection at an entrained flow reactor system and 50-MW coal-fired power plant in China. *J. Cleaner Prod.* **2021**, *287*, 124998.

(19) Rumayor, M.; Svoboda, K.; Švehla, J.; Pohořelý, M.; Šyc, M. Mitigation of gaseous mercury emissions from waste-to-energy facilities: Homogeneous and heterogeneous Hg-oxidation pathways in presence of fly ashes. *J. Emerg. Manage.* **2018**, *206*, 276−283.

(20) Raj, D.; Maiti, S. K. Sources, bioaccumulation, health risks and remediation of potentially toxic metal(loid)s (As, Cd, Cr, Pb and Hg): an epitomised review. *Environ. Monit. Assess.* **2020**, *192*, 1−20.

(21) Dai, B.; Zhang, A.; Liu, Z.; Wang, T.; Li, C.; Zhang, C.; Li, H.; Liu, Z.; Zhang, X. Facile synthesis of metallic Bi deposited BiOI composites with the aid of EDTA-2Na for highly efficient Hg^0 removal. *Catal. Commun.* **2018**, *121*, 53−56.

(22) Trobajo, J. R.; Antuña-Nieto, C.; Rodríguez, E.; García, R.; López-Antón, M. A.; Martínez-Tarazona, M. R. Carbon-based sorbents impregnated with iron oxides for removing mercury in energy generation processes. *Energy* **2018**, *159*, 648−655.

(23) Fernández-Miranda, N.; Lopez-Anton, M. A.; Díaz-Somoano, M.; Martínez-Tarazona, M. R. Mercury oxidation in catalysts used for selective reduction of NO_x (SCR) in oxy-fuel combustion. *Chem. Eng. J.* **2016**, *285*, 77−82.

(24) Yang, J.; Xu, H.; Zhao, Y.; Li, H.; Zhang, J. Mercury Removal from Flue Gas by Noncarbon Sorbents. *Energy Fuels* **2021**, *35*, 3581−3610.

(25) Liu, Y.; Liu, L.; Wang, Y. A Critical Review on Removal of Gaseous Pollutants Using Sulfate Radical-based Advanced Oxidation Technologies. *Environ. Sci. Technol. Lett.* **2021**, *55*, 9691−9710.

(26) Yang, Y.; Liu, J.; Liu, F.; Wang, Z.; Miao, S. Molecular-level insights into mercury removal mechanism by pyrite. *J. Hazard. Mater.* **2018**, *344*, 104−112.

(27) Wang, H.; Wang, S.; Duan, Y.; Li, Y.-n.; Ying, Z. Activated Carbon for Capturing Hg in Flue Gas under O_2/CO_2 Combustion Conditions. Part 2: Modeling Study and Adsorption Mechanism. *Energy Fuels* **2018**, *32*, 1907−1913.

(28) Liu, Y.; Shi, S.; Wang, Y. Removal of pollutants from gas streams using Fenton (-like)-based oxidation systems: A review. *J. Hazard. Mater.* **2021**, *416*, 125927.

(29) Sarafraz, M. M.; Pourmehran, O.; Yang, B.; Arjomandi, M. Assessment of the thermal performance of a thermosyphon heat pipe using zirconia-acetone nanofluids. *Renewable Energy* **2019**, *136*, 884−895.

(30) Liu, Z.; Adewuyi, Y. G.; Shi, S.; Chen, H.; Li, Y.; Liu, D.; Liu, Y. Removal of gaseous Hg^0 using novel seaweed biomass-based activated carbon. *Chem. Eng. J.* **2019**, *366*, 41−49.

(31) Pudasainee, D.; Gupta, R.; Khan, A. Performance Evaluation of Functionalized Biocarbon for Mercury Capture. *Energy Fuels* **2019**, *33*, 5867−5874.

(32) Wu, J.; Wang, H.; Shen, H.; Shen, C.; Zhu, Y.; Wu, J.; Ran, H. Experimental and Kinetic Analysis of H_2O on Hg^0 Removal by Sorbent Traps in Oxy-combustion Atmosphere. *Ind. Eng. Chem. Res.* **2021**, *60*, 12200−12209.

(33) Zhao, W.; Geng, X.; Lu, J.; Duan, Y.; Liu, S.; Hu, P.; Xu, Y.; Huang, Y.; Tao, J.; Gu, X. Mercury removal performance of

https://doi.org/10.1021/acsomega.1c06038
ACS Omega 2021, 6, 35124−35133

brominated biomass activated carbon injection in simulated and coal-fired flue gas. *Fuel* **2021**, *285*, 119131.
(34) Wang, H.; Shen, H.; Shen, C.; Li, Y.-n.; Ying, Z.; Duan, Y. Kinetics and Mechanism Study of Mercury Adsorption by Activated Carbon in Wet Oxy-Fuel Conditions. *Energy Fuels* **2019**, *33*, 1344−1353.
(35) Shen, H.; Wang, H.; Shen, C.; Wu, J.; Zhu, Y.; Shi, W.; Zhang, X.; Ying, Z. Effect of atmosphere of SO_2 coexisted with oxidizing gas on mercury removal under oxy-fuel condition. *Chemosphere* **2020**, *259*, 127525.
(36) Yang, L.; Wu, J.; Li, B.; Liu, D. Defective molybdenum disulfide nanosheet for elemental mercury capture in simulated flue gas. *J. Energy Inst.* **2021**, *94*, 120−128.
(37) Zhong, L.; Li, W.; Zhang, Y.; Norris, P.; Cao, Y.; Pan, W.-P. Kinetic studies of mercury adsorption in activated carbon modified by iodine steam vapor deposition method. *Fuel* **2017**, *188*, 343−351.
(38) Ghasemi, S. S.; Hadavifar, M.; Maleki, B.; Mohammadnia, E. Adsorption of mercury ions from synthetic aqueous solution using polydopamine decorated SWCNTs. *J. Water Process. Eng.* **2019**, *32*, 100965.
(39) Stavropoulos, G. G.; Samaras, P.; Sakellaropoulos, G. P. Effect of activated carbons modification on porosity, surface structure and phenol adsorption. *J. Hazard. Mater.* **2008**, *151*, 414−421.
(40) Zhou, Q.; Zhou, J.; Cao, H.; Xu, X. Effects of CO and CO_2 on the Removal of Elemental Mercury over Carbonaceous Surfaces. *ACS Omega* **2021**, *6*, 2916−2924.
(41) Xu, W.; Pan, J.; Fan, B.; Liu, Y. Removal of gaseous elemental mercury using seaweed chars impregnated by NH_4Cl and NH_4Br. *J. Cleaner Prod.* **2019**, *216*, 277−287.
(42) Zhou, Q.; Duan, Y.-F.; Hong, Y.-G.; Zhu, C.; She, M.; Zhang, J.; Wei, H.-Q. Experimental and kinetic studies of gas-phase mercury adsorption by raw and bromine modified activated carbon. *Fuel Process. Technol.* **2015**, *134*, 325−332.
(43) Yang, W.; Liu, Z.; Xu, W.; Liu, Y. Removal of elemental mercury from flue gas using sargassum chars modified by NH_4Br reagent. *Fuel* **2018**, *214*, 196−206.
(44) Gao, Z.; Liu, X.; Li, A.; Ma, C.; Li, X.; Ding, X.; Yang, W. Adsorption behavior of mercuric oxide clusters on activated carbon and the effect of SO_2 on this adsorption: a theoretical investigation. *J. Mol. Model.* **2019**, *25*, 1−11.
(45) Hsu, C.-J.; Chiou, H.-J.; Chen, Y.-H.; Lin, K.-S.; Rood, M. J.; Hsi, H.-C. Mercury adsorption and re-emission inhibition from actual WFGD wastewater using sulfur-containing activated carbon. *Environ. Res.* **2019**, *168*, 319−328.
(46) Chen, J.; Zhu, W.; Chang, X.; Ding, D.; Zhang, T.; Zhou, C.; Wu, H.; Yang, H.; Sun, L. DFT insights to mercury species mechanism on pure and Mn doped Fe_3O_4(111) surfaces. *Appl. Surf. Sci.* **2020**, *514*, 145876.
(47) Yang, Y.; Wang, Z.; Miao, S.; Liu, J.; Yu, Y.; Ding, J. Mechanistic Landscape of HCl-Mediated Hg^0 Capture by Magnetite. *J. Phys. Chem. C* **2019**, *123*, 30434−30442.
(48) Li, G.; Wang, S.; Wang, F.; Wu, Q.; Tang, Y.; Shen, B. Role of inherent active constituents on mercury adsorption capacity of chars from four solid wastes. *Chem. Eng. J.* **2017**, *307*, 544−552.
(49) Miklavcic, S. J.; Fung, C. Quantifying the force between mercury and mica across an ionic liquid using white light interferometry. *J. Colloid Interface Sci.* **2019**, *538*, 218−227.
(50) Xu, Y.; Luo, G.; Zhou, M.; Zhang, Q.; Li, Z.; Zhang, S. Natural ferruginous manganese ore for efficient immobilization of elemental mercury from coal combustion flue gas. *Fuel* **2021**, *283*, 118946.
(51) Hong, D.; Zhou, J.; Hu, C.; Zhou, Q.; Mao, J.; Qin, Q. Mercury removal mechanism of AC prepared by one-step activation with $ZnCl_2$. *Fuel* **2019**, *235*, 326−335.
(52) Wang, F.; Wang, R.; Jia, T.; Wu, J.; Xu, C.; Sun, Y.; Wang, X.; Wu, W.; Qi, Y. Spherical-shaped CuS modified carbon nitride nanosheet for efficient capture of elemental mercury from flue gas at low temperature. *J. Hazard. Mater.* **2021**, *415*, 125692.
(53) Yang, J.; Zhao, Y.; Guo, X.; Li, H.; Zhang, J.; Zheng, C. Removal of elemental mercury from flue gas by recyclable CuCl2 modified magnetospheres from fly ash. Part 4. Performance of sorbent injection in an entrained flow reactor system. *Fuel* **2018**, *220*, 403−411.
(54) Tang, H.; Li, C.; Duan, Y.; Zhu, C.; Cai, L. Combined experimental and theoretical studies on adsorption mechanisms of gaseous mercury(II) by calcium-based sorbents: The effect of unsaturated oxygen sites. *Sci. Total Environ.* **2019**, *656*, 937−945.
(55) Park, J.-H.; Wang, J. J.; Xiao, R.; Pensky, S. M.; Kongchum, M.; Delaune, R. D.; Seo, D.-C. Mercury adsorption in the Mississippi River deltaic plain freshwater marsh soil of Louisiana Gulf coastal wetlands. *Chemosphere* **2018**, *195*, 455−462.
(56) Zhang, J.; Duan, Y.; Zhou, Q.; Zhu, C.; She, M.; Ding, W. Adsorptive removal of gas-phase mercury by oxygen non-thermal plasma modified activated carbon. *Chem. Eng. J.* **2016**, *294*, 281−289.
(57) Ji, Q.; Luo, G.; Shi, M.; Zou, R.; Fang, C.; Xu, Y.; Li, X.; Yao, H. Acceleration of the reaction of H_2S and SO_2 by non-thermal plasma to improve the mercury adsorption performance of activated carbon. *Chem. Eng. J.* **2021**, *423*, 130144.
(58) Liu, Y.; Wang, Y. Elemental mercury removal from flue gas using heat and Co^{2+}/Fe^{2+} coactivated oxone oxidation system. *Chem. Eng. J.* **2018**, *348*, 464−475.
(59) Sriram, V.; Li, C.; Liu, Z.; Jafari, M.; Lee, J.-Y. Reaction kinetic study of elemental mercury vapor oxidation with $CuCl_2$. *Chem. Eng. J.* **2018**, *343*, 244−257.
(60) Li, Y.; Liu, Y.; Yang, W.; Liu, L.; Pan, J. Adsorption of elemental mercury in flue gas using biomass porous carbons modified by microwave/hydrogen peroxide. *Fuel* **2021**, *291*, 120152.
(61) Quirós-Álvarez, M.; Díaz Somoano, M.; Bongartz, W.; Vinjarapu, S. Mercury Interaction on Modified Activated Carbons under Oxyfuel Combustion Conditions. *Energy Fuels* **2018**, *32*, 5405−5408.
(62) Saleh, T. A.; Tuzen, M.; Sarı, A. Polyamide magnetic palygorskite for the simultaneous removal of Hg (II) and methyl mercury; with factorial design analysis. *J. Emerg. Manage.* **2018**, *211*, 323−333.
(63) Zhou, Q.; Duan, Y.; Chen, M.; Liu, M.; Lu, P.; Zhao, S. Effect of flue gas component and ash composition on elemental mercury oxidation/adsorption by NH_4Br modified fly ash. *Chem. Eng. J.* **2018**, *345*, 578−585.
(64) Duan, Y.; Duan, L.; Wang, J.; Anthony, E. J. Observation of simultaneously low CO, NO_x and SO_2 emission during oxycoal combustion in a pressurized fluidized bed. *Fuel* **2019**, *242*, 374−381.
(65) Li, Z.; Sun, D.; Chi, J.; Zhao, S. Efficient mercury removal at low temperature in flue gas with metal-organic frameworks modified by iodine. *Colloids Surf., A* **2021**, *626*, 126983.
(66) Guo, Y.; Tan, C.; Wang, P.; Sun, J.; Yan, J.; Li, W.; Zhao, C.; Lu, P. Kinetic study on CO_2 adsorption behaviors of amine-modified co-firing fly ash. *J. Taiwan Inst. Chem. Eng.* **2019**, *96*, 374−381.
(67) Skodras, G.; Diamantopoulou, I.; Pantoleontos, G.; Sakellaropoulos, G. P. Kinetic studies of elemental mercury adsorption in activated carbon fixed bed reactor. *J. Hazard. Mater.* **2008**, *158*, 1−13.
(68) Wang, S.; Li, H. Dye adsorption on unburned carbon: Kinetics and equilibrium. *J. Hazard. Mater.* **2005**, *126*, 71−77.

https://doi.org/10.1021/acsomega.1c06038
ACS Omega 2021, 6, 35124−35133